Evaluation of the Surface Wind Field over Land in WRF Simulations of Hurricane Wilma (2005). Part I: Model Initialization and Simulation Validation

DAVID S. NOLAN,[a] BRIAN D. MCNOLDY,[a] AND JIMMY YUNGE[a]

[a] *Rosenstiel School of Marine and Atmospheric Science, University of Miami, Miami, Florida*

(Manuscript received 16 June 2020, in final form 18 November 2020)

ABSTRACT: Although global and regional dynamical models are used to predict the tracks and intensities of hurricanes over the ocean, these models are not currently used to predict the wind field and other impacts over land. This two-part study performs detailed evaluations of the near-surface, overland wind fields produced in simulations of Hurricane Wilma (2005) as it traveled across South Florida. This first part describes the production of two high-resolution simulations using the Weather Research and Forecasting (WRF) Model, using different boundary layer parameterizations available in WRF: the Mellor–Yamada–Janjić (MYJ) scheme and the Yonsei University (YSU) scheme. Initial conditions from the Global Forecasting System are manipulated with a vortex-bogusing technique to modify the initial intensity, size, and location of the cyclone. It is found possible through trial and error to successfully produce simulations using both the YSU and MYJ schemes that closely reproduce the track, intensity, and size of Wilma at landfall. For both schemes the storm size and structure also show good agreement with the wind fields diagnosed by H*WIND and the Tropical Cyclone Surface Wind Analysis. Both over water and over land, the YSU scheme has stronger winds over larger areas than does the MYJ, but the surface winds are more reduced in areas of greater surface roughness, particularly in urban areas. Both schemes produced very similar inflow angles over land and water. The overland wind fields are examined in more detail in the second part of this study.

KEYWORDS: Boundary layer; Hurricanes/typhoons; Mesoscale models; Model evaluation/performance

1. Introduction

a. Motivation

In the present day, dynamical models that simulate global and regional weather are the primary tools for predicting the paths, intensities, and effects of hurricanes. For each hurricane, meteorologists at the U.S. National Hurricane Center (NHC) use forecasts from both global models and regional models to not only predict the maximum surface winds (defined as the maximum 1-min mean winds at 10 m elevation), but also the radial extent of the 64, 50, and 35 kt (1 kt $\approx 0.51\ \mathrm{m\ s^{-1}}$) winds in each of the northeast, southeast, southwest, and northwest quadrants. Extensive efforts are made to validate and improve these forecasts of wind speed and the size of the wind field (Gall et al. 2013; Sampson and Knaff 2015; Sampson et al. 2018).

However, these validation efforts have been almost entirely confined to hurricane winds over the ocean. In fact, unlike the wind speeds predicted for daily weather forecasts, or even in the cases of significant weather associated with strong midlatitude cyclones, output from global models or even hurricane forecast models are not used to predict wind speeds over land. Rather, overland decay models are used to guide forecaster intensity predictions over land, and local forecast offices issue wind forecasts based on the predicted track, intensity, and to some extent, size of the storm. The tropical cyclone wind speed probabilities products issued by NHC since 2006 do provide some guidance as to the expected wind speeds at inland locations (DeMaria et al. 2013).

A reluctance to issue specific wind forecasts over land based on model output is understandable for two reasons. First, as of 2018, 24- and 48-h track errors of the better forecast models are about 34 n mi (63 km) and 64 n mi (119 km), respectively (Cangialosi 2020). The areas of strong winds caused by hurricanes over land (e.g., sustained hurricane force) are of similar or even smaller scales (Powell et al. 1991; Powell and Houston 1996; Landsea et al. 2004). Therefore, errors in overland wind forecasts are likely to have large errors that depend at least as much on track forecasts as intensity forecasts. Second, there has been, to our knowledge, almost no validation of overland wind speeds from hurricane forecast models on a point-by-point basis.

Nonetheless, both track forecasts and intensity forecasts have been improving steadily for the last 30 years (Gall et al. 2013; DeMaria et al. 2013), and, perhaps optimistically, we can imagine a time in the not-too-distant future when hurricane forecast models have sufficiently accurate track, size, and intensity forecasts to provide useful point forecasts of expected peak wind speeds at coastal and inland locations. For inland locations, an additional effort is required: the evaluation and improvement of boundary layer and surface layer parameterizations for tropical storm and hurricane conditions over land.

This paper and its companion paper Nolan et al. (2021, hereinafter Part II) represent an effort to evaluate the potential for hurricane-specific dynamical models to predict wind speeds at inland locations, not just in terms of the maximum wind at any one time, but also in terms of the areal extents of hurricane force and tropical storm force winds over land. Furthermore, we consider the roles of planetary boundary layer

Corresponding author: Prof. David S. Nolan, dnolan@rsmas.miami.edu

DOI: 10.1175/MWR-D-20-0199.1

parameterizations and their embedded surface layer parameterizations to produce surface winds that are consistent with observations. To reduce to the greatest extent possible the influence of errors in track, intensity, and size, we use highly controlled simulations (not forecasts) of a landfalling hurricane. The initial and boundary conditions are manipulated so as to produce short-term simulations that produce center positions, peak wind speeds, radii of maximum winds (RMWs), and overall structural evolutions as similar to the real storm as possible.

The present papers are similar to the previous two part study by Nolan et al. (2009a,b). A variety of observational datasets obtained in Hurricane Isabel (2003) were used to evaluate how well the cyclone structure and surface wind field over the ocean were reproduced by two widely used boundary layer parameterizations: the Yonsei University (YSU; Hong et al. 2006) and the Mellor–Yamada–Janjić (MYJ; Janjić 1994) schemes. Nolan et al. used the Weather Research and Forecasting (WRF) Model and initial and boundary conditions from the Geophysical Fluid Dynamics Laboratory (GFDL) Hurricane Prediction System to produce 3-day simulations of Isabel as it moved across the central Atlantic as a category-5 hurricane. The simulations used three nested domains with the inner two nests following the cyclone center, and the inner nest grid spacing was 1.33 km. They found that both schemes reproduced the overall structure of the inner core, the boundary layer, and the surface wind field remarkably well. However, they did find that the MYJ scheme caused greater loss of angular momentum into the ocean, leading to overly strong inflow and an exaggerated secondary circulation as compared with the available observations.

A few previous studies have examined overland intensities and wind speeds of simulated hurricanes over land. Zhu (2008a,b) used the WRF Model and the MYJ scheme to simulate the landfalls of Hurricane Wilma (2005) and Hurricane Ivan (2004), respectively. These simulations used multiple nested grids to allow for very small horizontal grid spacings over small areas, but unlike most hurricane modeling studies that use vortex-following nests, the nested grids were fixed, with the smallest and finest grids placed over land. Zhu (2008a) found that the overall intensity of the simulated Wilma declined over land, as expected, and declined even faster if the land surface roughness was arbitrarily increased to higher values. However, the peak transient wind speeds on the inner most grid with grid spacing of 556 m, perhaps representative of wind gusts, did not decline in the simulations with increased roughness. Zhu (2008a) concluded that overland wind gusts can be more damaging that what is expected from the representative intensity because increased surface roughness generates more intense coherent structures in the boundary layer. A similar finding was reported for large-eddy simulations of idealized tornadoes by Nolan et al. (2017). In Zhu (2008b), the inner most grid had even smaller grid spacings of 100 m. With this resolution, and with the PBL scheme deactivated, horizontal rolls with scales ranging from a few hundred meters to a few kilometers appear in the innermost domain. Based on explicit calculations of eddy fluxes of heat and momentum caused by these rolls, Zhu argued that PBL schemes generally underestimate turbulent fluxes in hurricane conditions.

While Zhu focused on small-scale processes in the boundary layer, Lin et al. (2010) performed a broader assessment of the accuracy and utility of simulated landfall winds and precipitation, in this case using the example of Hurricane Isabel (2003) in North Carolina and Virginia. Lin et al. also used the WRF Model with fixed grids nested down to 1.33-km resolution and initialized from both Global Forecasting System (GFS) and GFDL analyses. To demonstrate that the simulated wind field was sufficiently realistic before landfall, Lin et al. compared the simulated wind fields with surface winds from the real time analysis system known as H*WIND (Powell et al. 1998; discussed further below). For the wind fields at landfall and inland, they compared the model output with time series observations from surface stations, including high-frequency observations from the Florida Coastal Monitoring Program (FCMP) mobile towers (Balderrama et al. 2011) that were deployed near the coastline, and additional research-quality observations farther inland at locations such as Richmond, Virginia, and Baltimore, Maryland. Lin et al. found that the simulated surface wind fields were generally consistent with observations, although the model slightly overpredicted the winds at landfall, generally underpredicted the winds in the right quadrant, and failed to reproduce damaging winds associated with outer rainbands. Lin et al. also evaluated the rainfall distributions and storm surge predictions made by forcing a hydrodynamic model with the wind fields from their WRF simulations. These hazards were not reproduced as accurately as the wind speeds.

The present study will not examine rainfall or surge, but will otherwise follow the example set by Lin et al. in several aspects. We first produce a pair of WRF simulations that are as consistent as possible with the track, intensity (peak wind speeds), and size of Hurricane Wilma (2005) as it moved across South Florida on 24 October 2005. As in Nolan et al. (2009a,b), the YSU and MYJ boundary layer schemes will be used. The surface wind fields over land will be studied in detail, by comparison with surface observations (including those made by the same FCMP towers), by consideration of the effects of the varying land surface roughness as defined by the WRF land use dataset, and in consideration of the localized wind maxima produced by resolved mesoscale coherent structures embedded in the low-level flow. By comparing the modeled wind fields with observations at locations both near and far from the storm center, we will also evaluate the accuracies of the sizes and shapes of the simulated wind fields.

b. *Hurricane Wilma (2005)*

Had it occurred in most of the recorded hurricane seasons to date, Hurricane Wilma would have been the most historically significant hurricane of its year, and perhaps even for some decades. In 2005, however, three other hurricanes also made category-3 landfalls (Beven et al. 2008), of which Hurricane Katrina caused loss of life in tragic numbers and epic storm surge flooding from New Orleans to Mobile Bay (Knabb et al. 2005). In fact, many of the meteorological aspects of Hurricane Wilma surpass the more notorious 2005 storms such as Katrina and Rita (Pasch et al. 2006). After forming in the Western Caribbean Sea on 15 October, Wilma drifted to the southwest

for 2 days and slowly strengthened to a strong tropical storm. After this development period, Hurricane Wilma exhibited a period of extreme rapid intensification with the estimated maximum surface winds increasing from 55 kt at 0000 UTC 18 October to 160 kt at 1200 UTC 19 October. The estimated minimum surface pressure fell to 882 hPa, which remains as the lowest known surface pressure for an Atlantic Ocean hurricane; physical explanations of this intensification event are discussed in detail in several other papers (Chen et al. 2011; Chen and Zhang 2013). After an eyewall replacement cycle, Wilma weakened to a more modest category 4 and moved northwestward, making landfall on the island of Cozumel, Mexico, on 21 October. Wilma moved slowly across the northeastern Yucatan Peninsula, causing considerable damage along the way, and then entered the Gulf of Mexico on 23 October with sustained surface winds of 85 kt.

Our interest in Hurricane Wilma begins at this time. Although substantially weakened by a prolonged interaction with the peninsula, Wilma was still a large and fairly symmetric tropical cyclone. A strong upper-level trough and cold front approaching from the northwest created deep southwesterly flow that began to move Wilma quickly toward the northeast. Despite 20–25 kt of southwesterly wind shear (at least as diagnosed from global model analyses) Wilma reintensified steadily, reaching a second peak intensity of 110 kt before making landfall near Cape Romano in southwest Florida. The intensity was estimated to be 105 kt at landfall around 1030 UTC 24 October. At this time Wilma was moving to the northeast at about 20 kt (11 m s^{-1}), and accelerating, and it crossed the Florida peninsula in just 4.5 h, with the center exiting the eastern coastline at a point very close to West Palm Beach.

Although not known for extreme damages due to wind or surge, Hurricane Wilma brought hurricane conditions and even sustained hurricane-force winds to almost every part of coastal and inland South Florida. Sustained (1-min average) hurricane force winds were reliably reported at such disparate locations as the West Palm Beach airport (KPBI; 71 kt), the Pompano Beach airport (KPMP, about 10 mi northwest of Fort Lauderdale; 72 kt), and Opa-Locka airport (KOPF, about 6 mi north of Miami International Airport; 74 kt). Hurricane-force gusts were reliably reported at additional locations such as Fort Lauderdale International (KFLL; 86 kt) Miami International (KMIA; 80 kt), and Key West International (KEYW; 72 kt). Wilma caused extensive minor to moderate damage in nearly every part of South Florida, leading to widespread power outages that lasted up to 3 weeks in some neighborhoods. The total financial cost of damages associated with Wilma has been estimated at $19 billion, making it the fourth most costly hurricane in U.S. history at the time it occurred. After accounting for inflation and considering all storms through 2017, Wilma stands as the ninth most costly hurricane in U.S. history (National Hurricane Center 2018).

c. *Overview of Part I and Part II*

Part I of this series documents the implementation of the WRF Model, including its configurations, parameterizations, and initialization. Following Nolan et al. (2009a,b), results with the YSU and MYJ schemes are compared with observational analyses of cyclone track, intensity, and size. For analyses and comparisons of overland wind speeds, the concept of open exposure is discussed and applied to the model output.

Part II focuses on wind speeds and directions at fixed locations, with direct comparisons with observations from airports and research towers. Wind directions are evaluated in terms of inflow angles relative to the cyclone center. Vertical profiles of wind speed in the lower boundary are compared with vertical profiles estimated from velocity–azimuth display (VAD) analyses from Doppler radars at Miami and Key West, Florida (Giammanco et al. 2013). The overall results are summarized and discussed.

2. Model and initialization

a. *Model, domain, and parameterizations*

This study uses WRF, version 3.9.1.1 (Skamarock et al. 2008). Many aspects of the model configuration are identical or similar to those used in the production of the two ''hurricane nature runs'' by Nolan et al. (2013) and Nolan and Mattocks (2014). All simulations use a modestly sized outer domain with 288 × 256 grid points and 9 km grid spacing, and two nested domains with 240 × 240 grid points with 3-km grid spacing and 432 × 432 grid points with 1-km grid spacing. The geographical location of the outer domain and the relative sizes of the inner domains are shown in Fig. 1a. The inner nests move with the cyclone by following the minimum geopotential height of the 700-hPa pressure surface. The simulations use 60 model levels in the vertical with the same distribution as the nature-run simulations (see Fig. 2 of Nolan et al. 2013). The shortwave and longwave radiation tendencies are computed every 5 min using the RRTM-G parameterizations (Iacono et al. 2008). The WRF double-moment 6-class microphysics scheme (Hong et al. 2010) parameterization is used for microphysics and precipitation. Cumulus parameterization is activated on the outer (9 km) domain, but, unlike in the nature-run simulations, we use the modified Tiedtke cumulus parameterization (Gregory et al. 2000; Wang et al. 2007).

As noted in the introduction, simulations are performed with the YSU and MYJ parameterizations. Each of these rely on the Monin–Obukhov theory for surface fluxes and flow in the surface layer, but the formulations are somewhat different for each scheme. The MYJ scheme as it is available in WRF does not account for the leveling off of the surface drag coefficient (or equivalently, the roughness length) at high wind speeds that has been documented in many recent studies (e.g., Donelan et al. 2004; Powell et al. 2003; French et al. 2007; Takagaki et al. 2012; Bell et al. 2012; Curcic and Haus 2020). Following Nolan et al. (2009a), the same formula for the roughness length over water that is coded into the YSU scheme for hurricane conditions in WRF 3.9.1.1 was also coded into the MYJ scheme. The standard version of the MYJ scheme available with WRF includes a modification to the diagnosed 10-m wind speed that causes it to be insensitive to local values of surface roughness, as first noted by Cao and Fovell (2016).

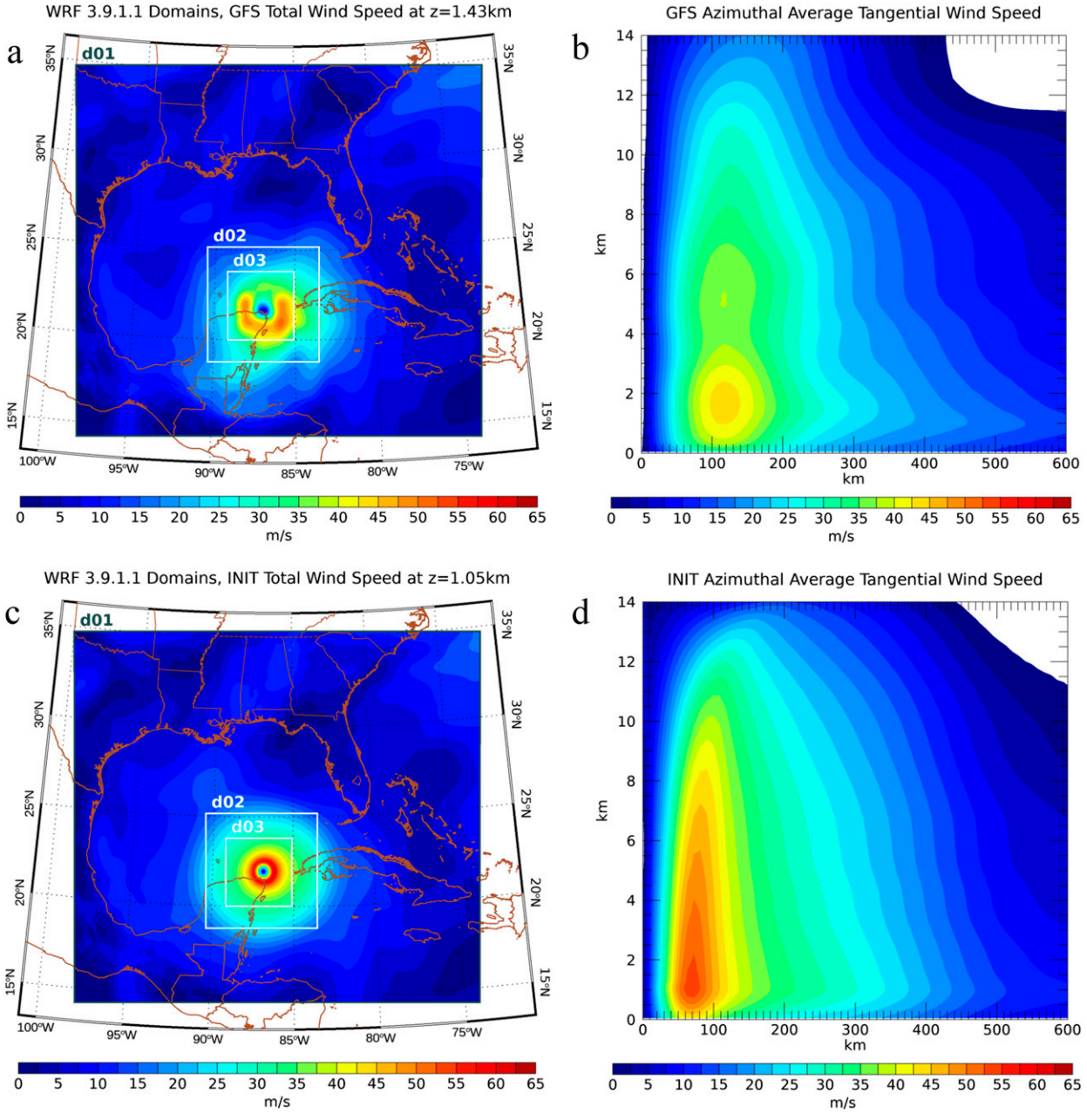

FIG. 1. WRF Model domain and initialization: (a) wind speed at $z = 1.43$ km at 0000 UTC 23 Oct from the GFS FNL analyses interpolated onto the WRF 9-km grid; (b) azimuthal-mean tangential wind for Hurricane Wilma at this time; (c) wind speed on the WRF grid after the vortex-bogusing procedure; (d) azimuthal-mean tangential wind speed for the bogus vortex.

Following their recommendation this modification was eliminated from the MYJ scheme.

To allow for ocean cooling, all simulations used the simple one-dimensional mixed-layer model of Pollard et al. (1973) that is available with WRF. As in Nolan et al. (2013), at all ocean points the mixed-layer depth was set to 25 m and the stratification at the bottom of the mixed layer was set to $0.2\,\mathrm{K\,m^{-1}}$. With these parameters the 1D model produces a cold wake behind and on the right side of the Nolan et al. nature-run hurricane with greatest reductions of sea surface temperature (SST) of about 2 K (not shown). Because of the fast forward motion of Hurricane Wilma, the simulated SST cooling within 100 km of the center is less than 0.2 K. These SST changes are realistic in comparison with observations and simulations of fast-moving hurricanes (D'Asaro et al. 2007; Yablonsky and Ginis 2009). The Noah Land Surface Model (Chen and Dudhia 2001; Ek et al. 2003; Alapaty et al. 2008), as it is implemented into WRF 3.9.1.1, is used to simulate surface temperatures and soil moisture over land.

b. Initial data, land use, and large-scale forcing

The large-scale wind, temperature, and humidity fields for the initial and boundary conditions are obtained from the Global Forecasting System (GFS) "FNL" analyses from 0000 UTC 23 October to 0000 UTC 25 October 2005. The initial SST, land surface, and soil layer temperatures were also taken from the GFS analyses. The land surface types were interpolated to the 9-km outer domain from the USGS 30″ dataset. An important capability of WRF, first introduced by Chen et al. (2007), is the run-time interpolation of higher-resolution land-use data (e.g., surface roughness, soil moisture) onto the 3- and 1-km nested grids as they move across the parent domain. This feature was used for all simulations. An additional minor change to the land surface data was made by modifying the surface roughness of the USGS "Wooded Wetland" land surface type from 0.4 to 0.2 m, which corresponds to the "Herbaceous Wetland" type. In the USGS dataset, most of the Everglades have the former designation, but in fact most of the Everglades corresponds to the latter type (Morris et al. 2019).

To ensure that the evolution of the large-scale environment and the path of the storm are as close to observations as possible, we use the analysis nudging technique that has been available in WRF since version 2.2 (Deng et al. 2007). The wind, temperature, and humidity fields at all model levels are relaxed (i.e., "nudged") toward the same fields from the GFS analyses interpolated in space to the grid points on the outer domain, and interpolated in time between the 6 h analyses. The large-scale nudging is only applied to the outer domain, and does not directly affect the data in the moving nests, except through the two-way interactions between the grids. Preliminary simulations found that a relaxation time scale of 12 h improved the track but that increasingly shorter times scales (i.e., stronger forcing) did not produce further improvement.

c. The vortex-bogusing technique

Even with the large-scale nudging activated, we find that a simulation that is simply initialized and forced with the GFS analyses does not produce satisfactorily accurate tracks and intensities for our study. To improve the outcome, we use the vortex-bogusing scheme developed by Rappin et al. (2013). The term "vortex bogusing" derives from the practice of removing a hurricane vortex from the initial state of a model and replacing it with a new vortex with a more correct location, size, and intensity—the so-called "bogus" vortex—in hopes of producing a more accurate forecast. The bogus vortex can be generated by another model (e.g., Kurihara et al. 1993; Hendricks et al. 2011) or it can be produced from a mix of analytical or empirical functions (e.g., Leslie and Holland 1995; Kwon and Cheong 2010). Rappin et al. use a vortex removal process that closely follows Kurihara et al. (1993, 1995), and the radial structure of the bogus vortex uses the modified Rankine (MR) vortex profile with a decay parameter a. The novel aspect of the Rappin et al. (2013) technique is to build the vertical structure of the vortex based on the maximum potential intensity theory of Emanuel (1986), following the formulation presented in Moon and Nolan (2010). This gives the initial wind field a realistic outward slope that increases with the size of the vortex (Stern and Nolan 2009).

Rappin et al. (2013) also developed a scheme to introduce a secondary circulation into the vortex; however, it did not satisfactorily improve the results. Rather, they found that simply increasing the specific humidity in the inner core by an arbitrary factor would accelerate the convection and the development of a realistic secondary circulation so that, after a 6–12-h adjustment period, the cyclone can achieve the correct intensity. The vertical and horizontal structure of this moisture enhancement is proportional to the normalized azimuthal-mean tangential wind speed V:

$$q_{\mathrm{enh}}(r,z) = q_{\mathrm{vap}}(r,z)\left[1 + E\frac{V(r,z)}{V_{\max}}\right], \tag{2.1}$$

where q_{vap} is the initial water vapor content, E is the enhancement factor, $V_{\max}$ is the peak tangential wind speed at any level, and q_{enh} is the adjusted water vapor. Values of 0.3 and 0.4 are used for E.

3. Track, intensity, and storm size

a. Preliminary simulations and final case selection

In our preliminary attempts at reproducing Hurricane Wilma, the WRF Model was initialized at 0000 UTC 23 October directly from the GFS analysis. This allows for 33 h of simulated evolution before the center made landfall. All preliminary simulations used the YSU boundary layer scheme. The NHC best-track analysis places Wilma at 21.6°N, 87.0°W, with maximum wind speed 85 kt (44 m s^{-1}), minimum surface pressure 960 hPa, a radius of maximum winds of 55 km, and a radius of gale force winds of 240 km (available from the Extended Best Track Dataset; Demuth et al. 2006). After interpolation of the GFS data to the WRF outer domain, the corresponding values at the initial time are 21.5°N, 86.9°W, 42.8 m s^{-1}, 977 hPa, 120 km, and 325 km. A horizontal view of the wind speed and a radius-height cross section of the azimuthally averaged tangential wind from the GFS at 0000 UTC are shown in Figs. 1a and 1b.

The track and intensity of this first simulation, labeled GFS, is shown in Fig. 2 along with one of the subsequent preliminary simulations, and also the final simulations. Here and in later analyses, the cyclone centers are computed using a pressure centroid method similar to that described by Nguyen et al. (2014): we find the centroid of the negative surface pressure anomaly in a 100 km × 100 km box that is initially centered at the center of the nested grid, and this procedure is iterated four more times with each updated box center being the outcome of the previous calculation.

Despite initialization of a cyclone that is too large, a bit weak, and not in the right location, the resulting 48 h simulation is very similar to the real storm. The track follows the best track very closely for the first 18 h but then travels on a path slightly south of the best-track positions until it rejoins the best track at 1200 UTC. While track and intensity of this first attempt were remarkably good, we did find that the RMW was a

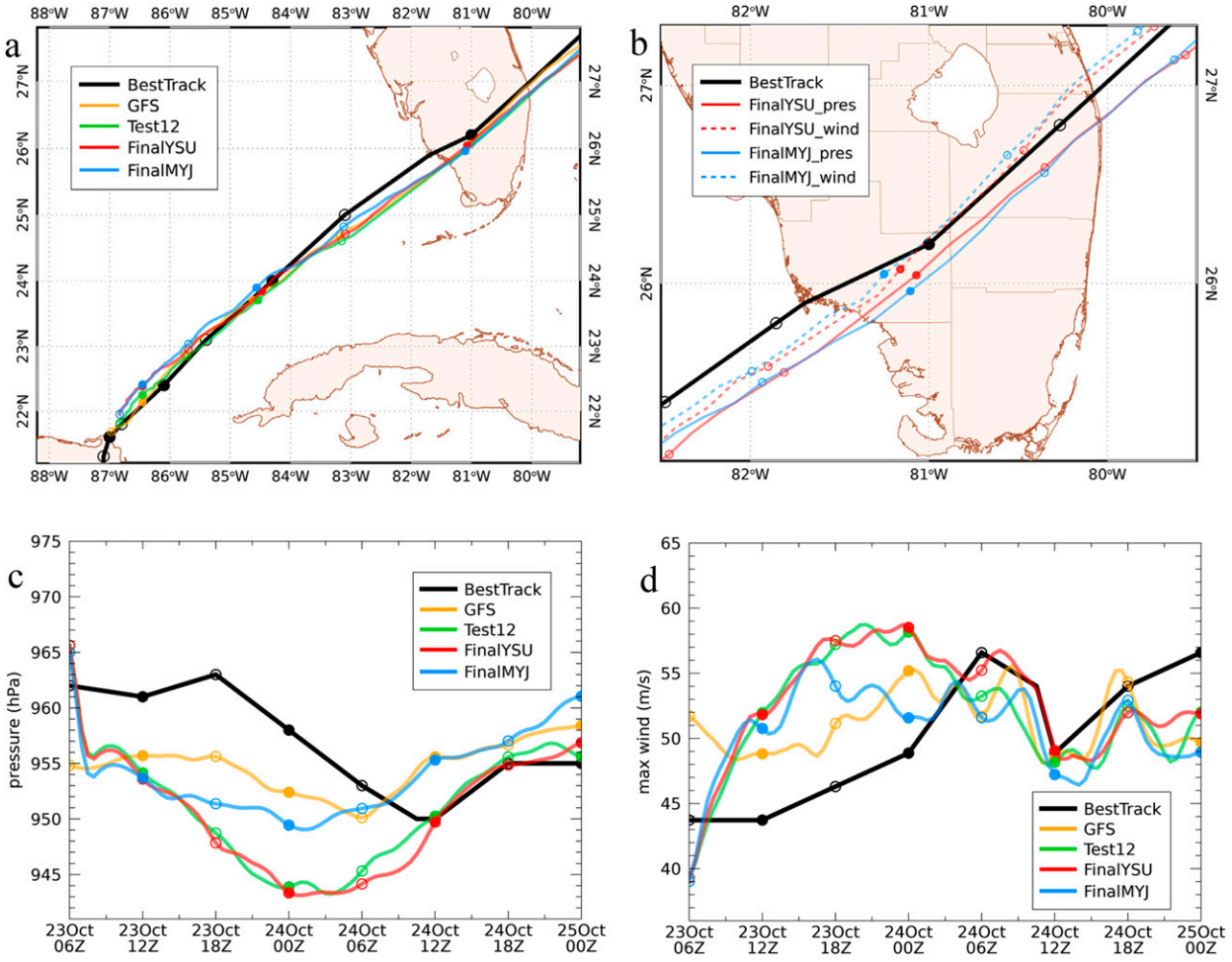

FIG. 2. Tracks and intensities for preliminary (GFS and Test 12) and final (FinalYSU and FinalMYJ) simulations of Hurricane Wilma (2005): (a) cyclone centers as defined by pressure centroid, with open symbols at 0600 and 1800 UTC and closed symbols at 0000 and 1200 UTC; (b) close up of tracks over Florida, showing pressure centroid centers (solid) and wind centers (dashed), with open symbols every 2 h and closed symbols at 1200 UTC; (c) minimum surface pressure; (d) maximum surface wind speed. The track and intensity data are taken from the 3-km grid every 30 min and smoothed in time.

bit larger and the azimuthal-mean wind speeds were a bit less than what is shown from observational analyses (not shown). Lin et al. (2010) also found the RMW to be too large for their simulations of Hurricane Isabel (2003) that were initialized from GFS data.

In an attempt to bring the intensity and structure of our simulated hurricane as close to the real Wilma as possible, we proceeded with modifications to the initial location, size, and intensity of the vortex. The process was one of trial and error, with each modification based on the relative success of the previous simulation. The input parameters for some of these test cases are shown in Table 1. The first change, labeled Test1, was to replace the GFS vortex with a bogus vortex designed to match the best-track position and other information from the extended best-track analysis. However, all simulations initialized at 0000 UTC with bogus vortices showed a significant southward shift of the track. We attempted to overcome this shift by relocating the initial vortex 0.1° or 0.2° to the north and/or west, but such modifications resulted in little improvement.

To improve the track, the start time for the simulations with vortex bogusing was changed to 0600 UTC 23 October. Using the extended best-track information as a guide, the bogus vortex was set to have $V_{max} = 56.5\,m\,s^{-1}$ at the top of the boundary layer, with a RMW of 81 km. While this is larger than the analyzed RMW of 30 n mi (55 km) at that time, we know from experience with the vortex-bogusing technique that the surface RMW usually becomes established at a smaller radius than the initially prescribed value. To overcome the initial spindown due to surface friction, the inner-core moisture enhancement was set to $E = 0.3$. This was case Test11, and while it produced a good track and intensity, its RMW was too large at landfall (not shown). To reduce the size of the wind field, case Test12 used an initial RMW of 63 km. Horizontal and vertical cross sections showing size of the initial vortex in this bogus vortex are shown in Figs. 1c and 1d. The results of this

TABLE 1. Input parameters for Wilma simulations.

Name	Start time (UTC 23 Oct)	Initial lat, lon	RMW (km)	MR decay parameter a	Moisture enhancement E	PBL scheme	Comments
GFS[a]	0000	21.5°N, 86.9°W	120	—	—	YSU	Too large and too weak at landfall
Test1	0000	21.6°N, 87.0°W	99	0.83	1.0	YSU	Too large and too far south at landfall
Test11	0600	21.8°N, 86.8°W	81	0.74	1.3	YSU	Good track; RMW too large
Test12	0600	21.8°N, 86.8°W	63	0.74	1.3	YSU	Landfall track too far south
FinalYSU	0600	22.0°N, 86.8°W	63	0.74	1.3	YSU	Best track and intensity
FinalMYJ	0600	22.0°N, 86.8°W	63	0.74	1.4	MYJ	Slightly weaker than FinalYSU

[a] Initial location and size are not prescribed but are estimated from GFS FNL analysis data.

simulation are shown in Fig. 2. The track of Test12 was still not quite as good as desired, so we again tried relocating the initial vortex. After additional tests, we found that moving the starting location of the vortex at 0600 UTC by 0.2° to the north produced a track that makes landfall and traverses Florida just slightly north (by just a few km) of Test12. This case was selected as the final simulation using the YSU scheme, and is hereinafter referred to as FinalYSU. When the same initial conditions were used with the MYJ boundary layer scheme, the result also had a very similar track, but the intensity was 3–5 m s^{-1} less than FinalYSU at the time of landfall. To increase the landfall intensity, the moisture enhancement factor E was changed to 0.4. This causes the intensity of FinalMYJ to be about 3 m s^{-1} stronger just before landfall, just below the values for FinalYSU and for the best track.

Minimum surface pressures and maximum surface wind speeds for these various cases are also shown in Fig. 2. Previous work has shown that maximum instantaneous wind speeds in WRF hurricane simulations on 1 km grids can exceed the equivalent 1-min mean winds by as much as 5% (Uhlhorn and Nolan 2012; Nolan et al. 2014). To mitigate this overestimation of wind speeds, the wind speed data in Fig. 2 is derived from the 3-km nested grid every 30 min. In addition, both the surface pressure and surface wind data have been smoothed in time over a 3-h interval around each data point.

As mentioned above, the centers shown in Fig. 2a are based on centroids of low pressure around the cyclone centers. Close inspection of this figure would indicate that all of these tracks remain south of the best track as the storm traverses Florida. However, the best-track positions are also influenced by centers based on the location of minimum wind speed (wind centers). Because of the storm motion, the wind center in a hurricane will generally be to the left of its pressure center. Figure 2b shows a close-up of the pressure-based tracks of FinalYSU and FinalMYJ, along with their wind centers. The wind center is computed from the location of minimum wind speed that is within 50 km of the pressure center, after the wind field has been smoothed 50 times with a 1–1–1 filter in both directions. These centers are closer to the best-track landfall point, are nearly on top of the 1200 UTC best-track location, and then move even farther north as the storm exits the east coast. Their increasing northward displacement is consistent with the increasing speed of the storm.

b. *Size and intensity before landfall*

For the purposes of this study the size of the wind field is as important as the peak wind speed. This is because we will be evaluating the surface wind field in the populated and urbanized areas along the Florida east coast, much of which was quite far from the cyclone center (e.g., Miami and Fort Lauderdale). Even if the peak surface wind speeds and minimum pressures match Wilma perfectly, if the simulated wind fields are too small or too large, the comparisons will not be useful.

To evaluate the sizes of the surface wind fields, we compare them with objectively analyzed wind fields from two very different techniques: H*WIND and the Tropical Cyclone Surface Wind Analysis (TCSWA). H*WIND (Powell and Houston 1996; Powell et al. 1998) was developed to produce near real-time analyses of the surface wind field based on all available wind speed observations, including flight-level winds from reconnaissance aircraft, but also using dropsondes, scatterometer measurements, surface instruments, and surface winds estimated from the Stepped Frequency Microwave Radiometer (SFMR; Uhlhorn et al. 2007). H*WIND uses cubic basis functions to construct a wind field with minimal deviation from the observations, thus producing its famously smooth and rounded contours.

TCSWA is a component of the more comprehensive Multiplatform Tropical Cyclone Surface Wind Analysis, which uses a combination of satellite, SFMR, and flight-level data (Knaff et al. 2011, 2015). For Wilma, only flight level data were available for this analysis. A significant difference from H*WIND is that TCSWA interpolates the data to a polar coordinate grid and uses different filtering weights in the radial and azimuthal directions, with half-power weights of 4 km and 70°, respectively, so that wind speed information at a given radius has a large influence on nearby points at the same radius but much less influence at different radii.

H*WIND analyses are available for Wilma at 0730 and 1230 UTC, while the TCSWA analyses are available at 0600 and 1200 UTC. Figure 3 shows the surface wind speed from FinalYSU and FinalMYJ at 0600 UTC and also the H*WIND and TCSWA analyses from their nearby times. The four plots

have many similarities, and many differences. All four show peak surface winds ranging from 50 to 60 m s^{-1}. The model fields, being instantaneous snapshots of high-resolution numerical simulations, show small-scale variations caused by a mixture of convective downdrafts and poorly resolved streamwise bands. Transient features with wind reaching 50 m s^{-1} appear in all quadrants for FinalYSU and FinalMYJ; however, both of these show broad areas of winds exceeding 50 m s^{-1} to the south and southeast of the center and broad areas of winds less than 40 m s^{-1} north and northeast of the center. These broader areas of higher winds are consistent with the locations of peak winds shown in the inherently smoother H*WIND and TCSWA analyses. The H*WIND analysis system produces a very smooth wind field, while the TCSWA analysis is quite choppy, perhaps because it is based only on flight level observations that are mostly limited to the paths of the standard "figure 4" flight pattern. The motion-induced asymmetries of the simulated winds fields are considerably less than for the analyses. The amplitude of the wave-number-1 asymmetry of the surface wind field around 0600 UTC, averaged in an annulus within 30 km of the RMW, is 9.1 m s^{-1} for H*WIND and 5.2 m s^{-1} for TCSWA but is only 3.2 m s^{-1} for FinalYSU and 1.3 m s^{-1} for FinalMYJ.

It might be possible to process the model output to produce a more "apples to apples" comparison with the observational analyses, perhaps either by smoothing the wind field, or by ingesting the model output into the objective analysis schemes (H*WIND and TCSWA). However, our reason for using the objective analyses is to evaluate the intensities and sizes of the simulated vortices as they approach and then cross over Florida. For this purpose we compute azimuthal-mean profiles of wind speed $V_{\rm tot}$, and tangential wind V_t and radial wind V_r relative to the vortex center, for the simulations and for H*WIND and TCSWA. For the model fields, the vortex center is defined by the same algorithm that was described in section 3a. The azimuthal-mean fields from the simulations are also composited in time, using model output from 0530, 0600, 0630, 0700, and 0730 UTC.

Radial profiles of $V_{\rm tot}$, V_t, and V_r for FinalYSU and FinalMYJ are shown in Figs. 3e and 3f, each with comparisons with H*WIND (at 0730) and TCSWA (at 0600). H*WIND analyzes a smaller and slightly stronger vortex with the RMW very close to the extended best-track value of 30 n mi (56 km) and with a peak mean $V_{\rm tot}$ near 46 m s^{-1}. TCSWA produces a broader and weaker vortex with peak $V_{\rm tot}$ only reaching 34 m s^{-1}. FinalYSU and FinalMYJ fall between these values, both with peak $V_{\rm tot}$ of 42 m s^{-1}. The RMW is about 75 km for FinalYSU and TCSWA, whereas it is 90 km for FinalMYJ.

The simulations and the TCSWA profiles are quite similar to each other, but moving toward the cyclone center, both are starkly different from H*WIND. H*WIND produces radial profiles of V_t and V_r that are concave downward in a broad area around the RMW, and then transition to a linear decay close to $r = 0$, with both reaching zero at the exact center. The models and TCSWA produce maxima with sharper peaks that transition more quickly to linear decreases inside the RMW. While V_t and V_r for TCSWA also approach zero at $r = 0$, the model profiles somewhat "flatten" to values closer to zero at radii of 10–20 km. Nolan et al. (2013) argued that this behavior of the surface wind fields becoming very small in a nontrivial area around the vortex center is actually more realistic, because if radial winds do penetrate all the way to $r = 0$ at the TC center, mass conservation would require significant vertical motion at low levels in the eye, which is not observed. These differences in the size of the low-wind speed areas of the eyes are also evident in the plan view plots above. The dark blue areas, indicating wind speeds less than 10 m s^{-1}, are very similar in size for the simulations and TCSWA but are much smaller for H*WIND.

Unlike for H*WIND and TCSWA, $V_{\rm tot}$ for the simulations does not go to zero at the center, because the center is based on a pressure centroid and does not coincide with the minimum wind. V_t and V_r at the first radial grid point ($r = 1.5$ km) are not computed accurately. These anomalies could be eliminated by defining the TC center with location of minimum wind (instead of the pressure centroid), but this leads to a significant reduction in the peak winds, because Wilma was moving rapidly northeastward, and the wind minimum was considerably displaced from the pressure center. The H*WIND and TCSWA analyses specify the wind speed to be zero at the vortex center.

Additional confidence in the realism of the FinalYSU and FinalMYJ simulations can be provided by comparing their simulated reflectivities with observations. The left column of Fig. 4 shows the WSR-88D reflectivity from Key West (KBYX) at 0557 UTC along with simulated reflectivities at 0600 UTC from FinalYSU and FinalMYJ. The simulated reflectivities have many similarities to the observed, such as an elliptical shape of the eyewall with major axis from north-northwest to south-southeast, an enhancement of reflectivity on the northwest side of the eyewall, enhanced areas of precipitation southeast of the eyewall that are approaching Key West, and a broader area of precipitation (or perhaps a principal band) northeast of the storm. There are also some differences, most notably that the simulations generally have significantly higher reflectivity values in the convective areas, often exceeding 50 dBZ, whereas the observed values only reach 50 dBZ in the northern eyewall. At the same time, the radar shows almost all of the area near the storm filled in with lighter precipitation with 10–30 dBZ. This high-reflectivity bias has been seen in many previous hurricane simulations (Braun 2006; Rogers et al. 2007; Davis et al. 2008). The right column shows data from Miami (KAMX) at 1315 UTC, FinalYSU at 1430 UTC, and FinalMYJ at 1400 UTC. These times correspond to the passage of a boundary layer wind maximum over the KAMX site that will be discussed in Part II. Otherwise, the similarities and dissimilarities discussed above are still present. The echo-free eye regions over land are slightly larger in the simulations.

c. *A first look at overland wind speeds*

Figure 5a shows a snapshot of surface wind for FinalYSU at 1230UTC. The low-wind region of the eye is over land, surrounded by a noisy ring of surface winds reaching 30–35 m s^{-1}. The fastest surface winds occur over the ocean on both sides of the peninsula with speeds reaching 47 m s^{-1}. It is interesting to note how the winds over Lake Okeechobee are also increased relative to the surrounding land, with the wind speed increasing as it moves from east to west across the lake. Another

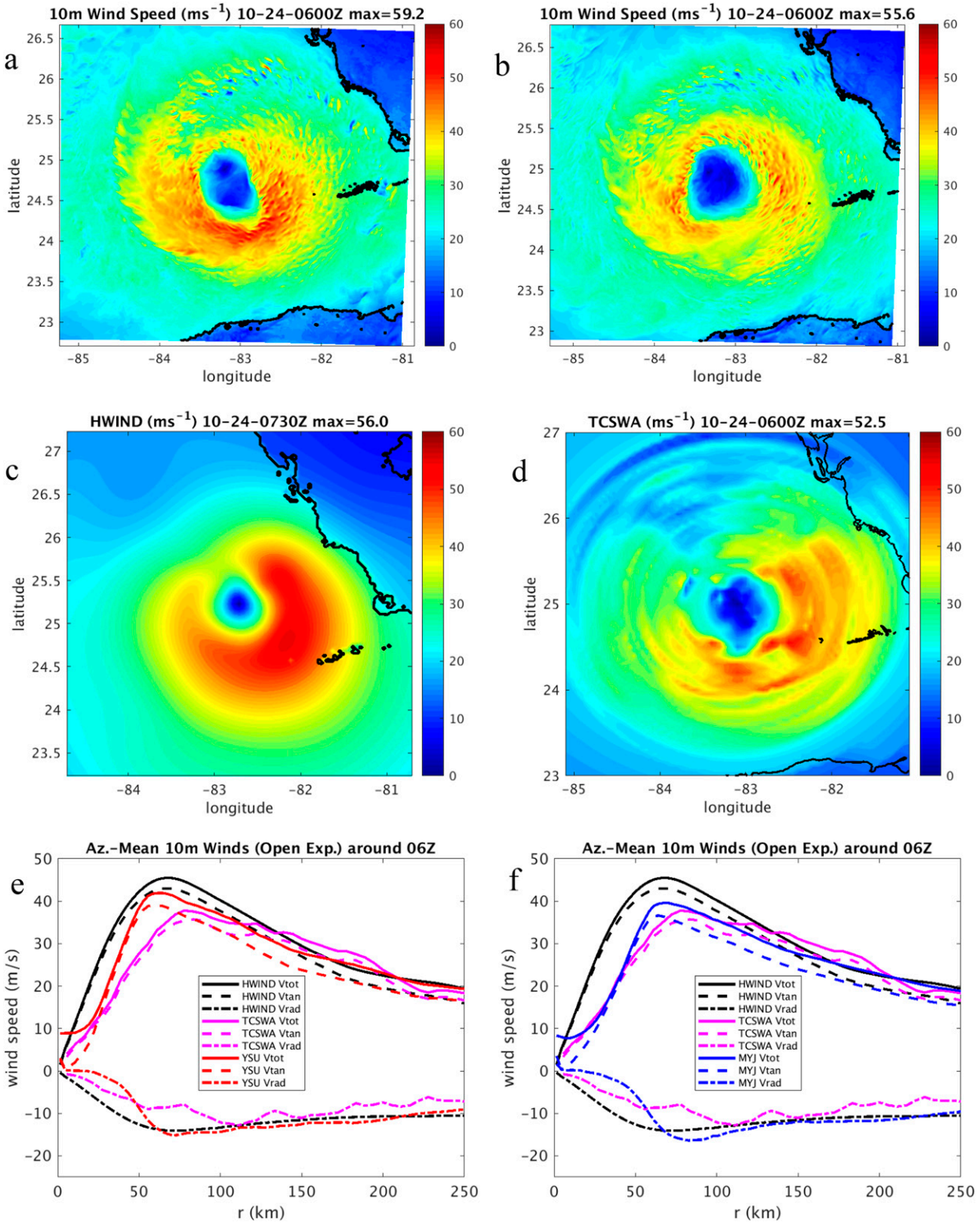

FIG. 3. Simulated and observed surface wind fields around 0600 UTC: surface wind speed for (a) FinalYSU and (b) FinalMYJ; (c) H*WIND analysis centered at 0730 UTC; (d) TCSWA analysis at 0600 UTC; azimuthal-mean profiles of total, tangential, and radial wind speeds for (e) YSU and (f) MYJ compared with the analyses.

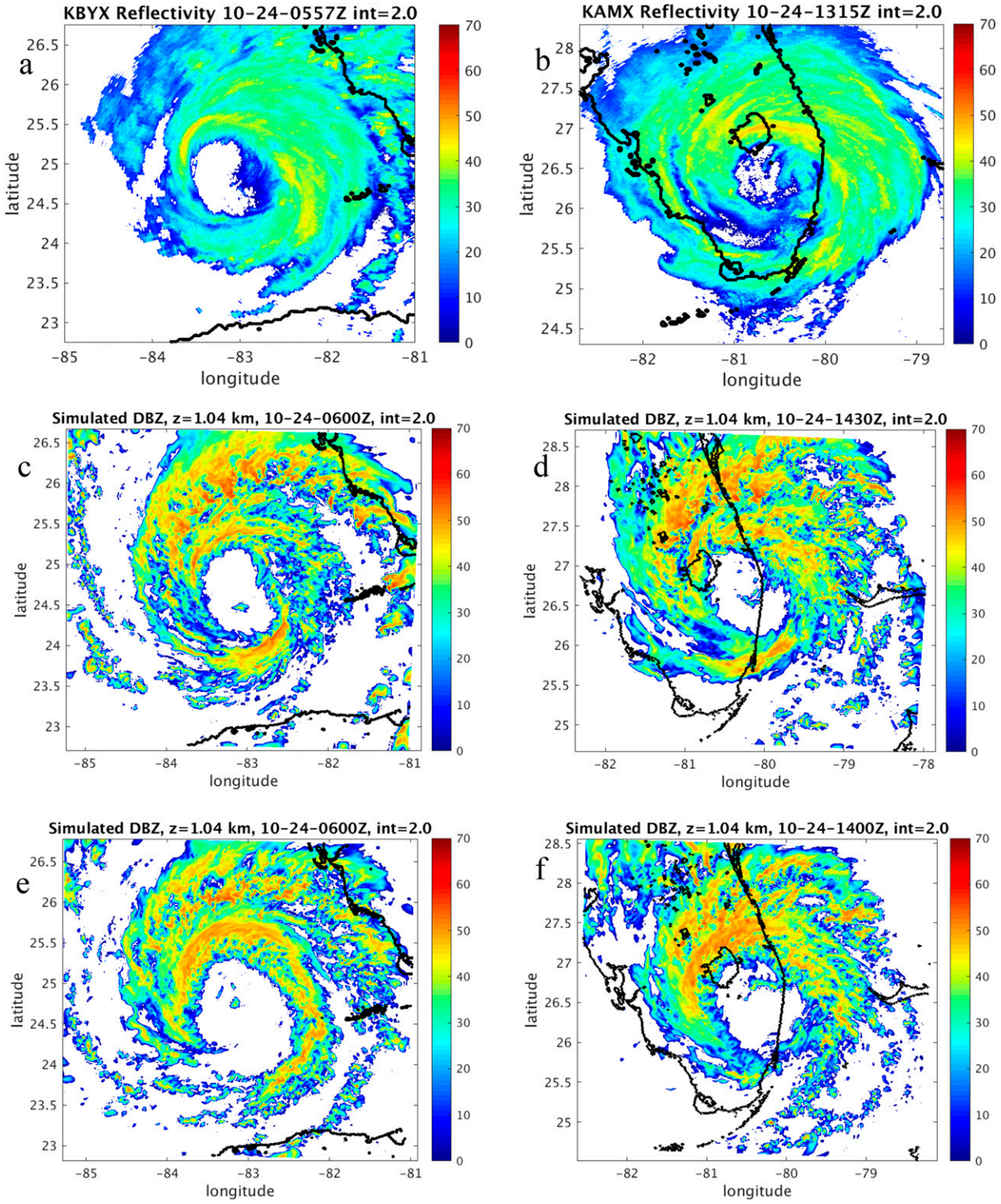

FIG. 4. Observed and simulated reflectivities before and during landfall: (a) observed from KBYX at 0557 UTC; (b) observed from KAMX at 1315 UTC; (c) FinalYSU at 0600 UTC; (d) FinalYSU at 1430 UTC; (e) FinalMYJ at 0600 UTC; (f) FinalMYJ at 1400 UTC.

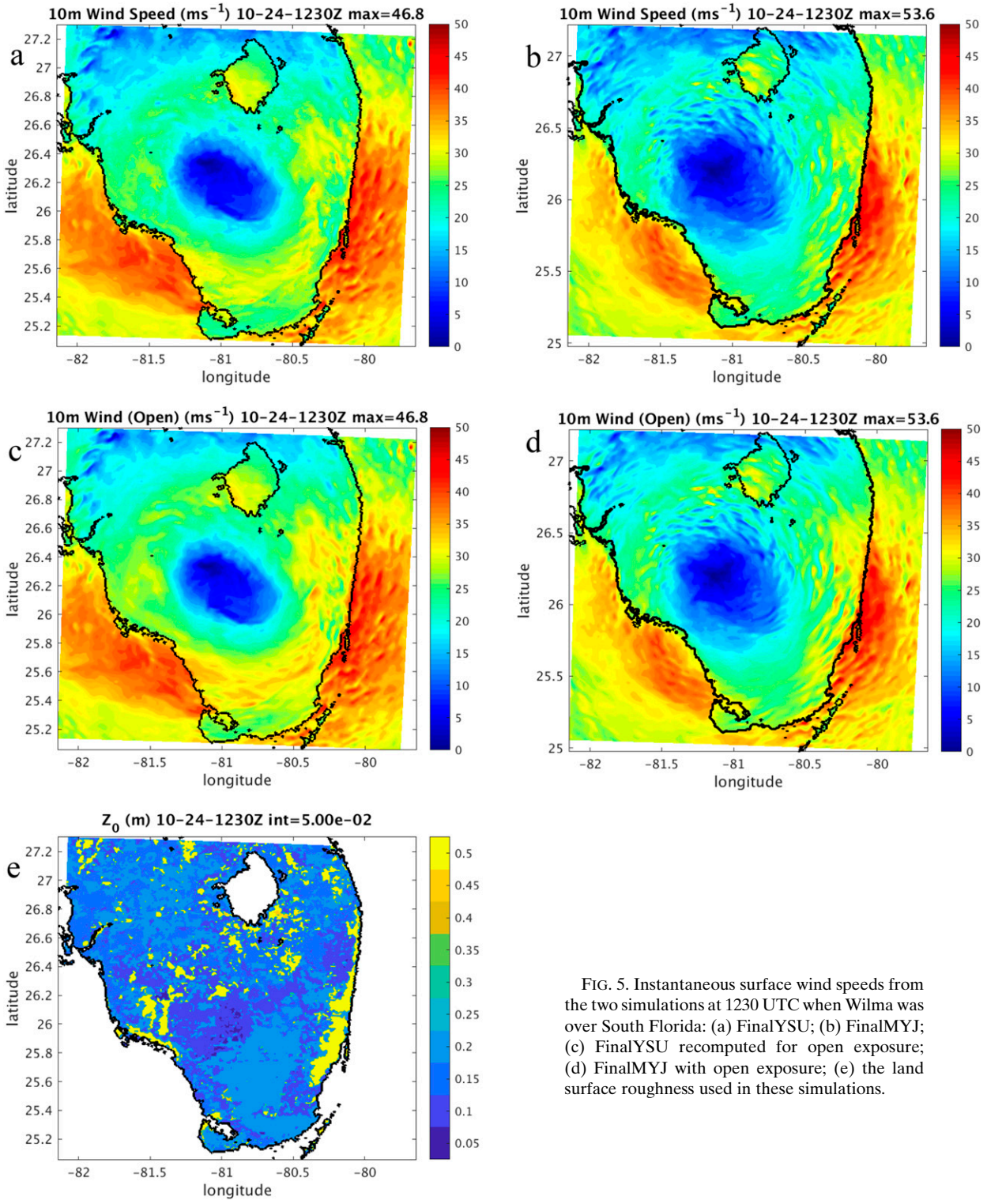

FIG. 5. Instantaneous surface wind speeds from the two simulations at 1230 UTC when Wilma was over South Florida: (a) FinalYSU; (b) FinalMYJ; (c) FinalYSU recomputed for open exposure; (d) FinalMYJ with open exposure; (e) the land surface roughness used in these simulations.

important feature that can be seen in Fig. 5a is a reduction in surface wind in the urban areas corresponding to the Miami and Fort Lauderdale metropolitan areas. This can be expected since the surface roughness $z_0 = 0.5$ m in these areas, which is the largest value in the WRF land use dataset. For reference, z_0 over South Florida is shown in Fig. 5e.

Figure 5b shows a similar snapshot for FinalMYJ. While similar in many ways to FinalYSU, the FinalMYJ wind field

has some interesting differences. Organized streaks of faster and slower winds are more prominent. The streaks are roughly parallel to concentric circles around the center, but this means that they are actually aligned at an angle radially outward from the near surface flow, which points inwards at angles of 20°–40° (to be shown below). This propensity of the MYJ scheme to produce streamwise wind streaks was also noted by Cohen et al. (2015) in their study of winter season convective environments in the southeastern United States. Another difference can be seen in the urban corridor: the FinalMYJ surface winds are reduced in this area, but not as consistently as for FinalYSU; the aforementioned wind streaks in FinalMYJ appear to be causing higher winds in the urban areas.

It is a common practice in meteorology and engineering to convert observed surface winds to an equivalent wind in an "open exposure" environment, as might be expected for the ideal setup such as an isolated tower in the middle of a large open area with no nearby obstructions, such as at an airport (Powell et al. 1996; Masters et al. 2010). This gives a more accurate description of the intensity of a wind event, as the same boundary layer wind profiles will produce different near-surface winds depending on the surrounding and upstream surface roughness relative to the point of observation. Furthermore, H*WIND analyses also correct for open exposure in the ingestion of surface wind measurements, and presume open exposure when generating the final analyses (e.g., for extrapolation of flight-level winds to the surface).

In WRF, zonal and meridional surface winds are not "state variables" that contribute to the dynamical evolution of the model. Rather, they are diagnosed at the end of each time step from the wind speed of the lowest model level, the surface roughness, and other factors such as the low-level stability. In theory, we should be able to exactly diagnose the open exposure wind speeds from the model output from a similar procedure, but using a different surface roughness z_{open}:

$$V_{open} = V_1 \times \frac{\log(10.0/z_{open})}{\log(h_1/z_{open})}, \tag{3.1}$$

where here we have neglected the effects of the stability function $\psi(z)$, h_1 is the height above ground of the lowest model level (ranging from 41 to 43 m in these simulations), and we would use $z_{open} = 0.03$ m (e.g., Masters et al. 2010).

However, some of the analyses in this study rely on model output of the surface fields every 10 s to more precisely compute 1- and 10-min mean winds. The three-dimensional wind fields were saved every 5 min, so the lowest model level data are only available at that frequency. Instead, we can use the surface wind and the logarithmic wind law to estimate the wind at the lowest model level and then reverse the formula, but using z_{open}, leading to

$$V_{open} = V_{10} \times \frac{\log(h_{ref}/z_0)}{\log(10/z_0)} \times \frac{\log(10/z_{open})}{\log(h_{ref}/z_{open})}, \tag{3.2}$$

where h_{ref} is a reference value that can be chosen to be equal to the lowest model level. Generally, open exposure wind speeds derived from (3.2) are nearly identical to those derived from the lowest model level using (3.1); the results using (3.2) are shown in Figs. 5c and 5d.

For FinalYSU, the open exposure correction increases the surface winds over all the land points. The urban area winds are increased the most, although they are still not as fast as the surrounding nonurban areas. This should be expected: the increased downward momentum flux in the urban areas also decreases the winds in the overlying boundary layer. In other words, an instrument placed in an area of open exposure, but surrounded by a larger urban environment, will experience reduced winds relative to an instrument in an entirely open environment. Open exposure also increases the winds over land for FinalMYJ, and also in the urban corridor. However, as noted above, the area of reduced winds is less distinct for FinalMYJ due to the wind streaks, and after correction, some of the fastest instantaneous wind speeds over land are occurring in the urban zones.

d. Size and intensity over land

Figure 6 shows larger views of the surface wind speeds and their azimuthal means around 1230 UTC, when Wilma was halfway through its traversal across Florida. Since the surface underneath the storm changes rapidly at this time, the azimuthal means are composited only using data from 1200, 1230, and 1300 UTC. For this comparison the correction for open exposure is used. TCSWA uses a very simple modification of the wind speed over land, decreasing the wind speed by an additional 20% and turning the inflow angle an additional 20° inward (J. Knaff, personal communication).

Much like over water, the simulated and analyzed wind fields have many differences, but they are also quite similar in some respects. Both FinalYSU and FinalMYJ show localized areas of winds over land exceeding 40 m s^{-1}, with FinalMYJ showing a few stronger wind maxima over land, but also less areal coverage of winds in the 30–35 m s^{-1} range. H*WIND shows a broad swath of winds exceeding 40 m s^{-1} over the eastern side of the peninsula, and another swath of winds reaching 35 m s^{-1} on the western side. TCSWA diagnoses a peak wind speed of 59 m s^{-1} just inside the eastern coastline, which is almost certainly anomalous, and possibly due to a mismatch in the position of the coastlines used by TCSWA and WRF.

Figure 6 also shows the azimuthal-mean profiles. The maximum azimuthal-mean winds are quite similar for all four profiles, ranging from 31 to 34 m s^{-1}. FinalYSU has the smallest RMW at 76 km, while the RMWs for H*WIND, FinalMYJ, and TCSWA are 80, 86, and 90 km, respectively. Although the extended best-track dataset reports 30 n mi (55 km) for the RMW at 1200 UTC, the same value as for 0600 UTC, it seems far more likely that the inner-core wind field expanded as the storm moved over land, as suggested by both analyses and both models.

e. Inflow angles

The azimuthal-mean profiles for FinalYSU, FinalMYJ, and TCSWA have similar shapes, not only in V_{tot}, but also in the decomposition into V_t and V_r, both over water and land. Over land, however, peak values of V_t and V_r for H*WIND are

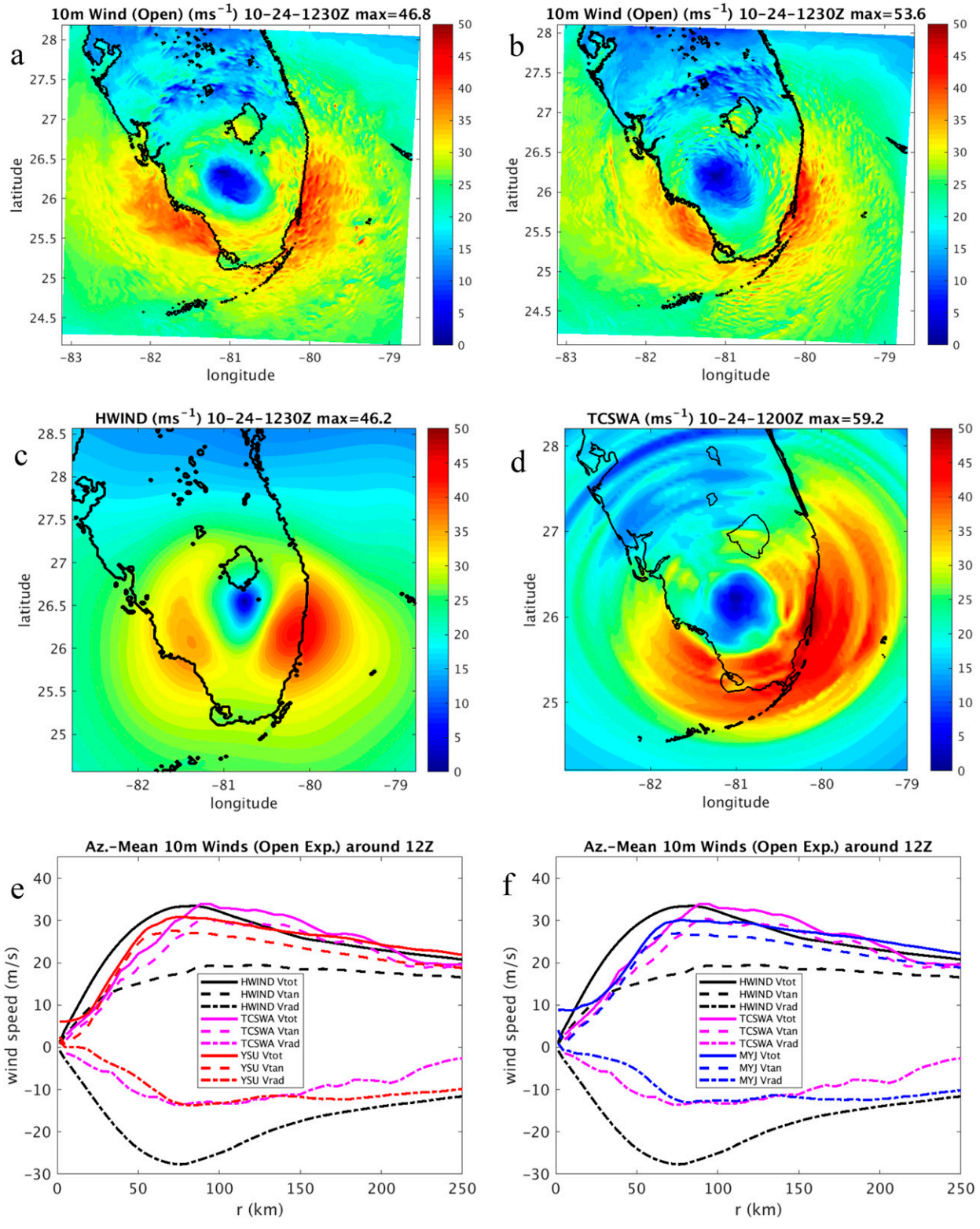

FIG. 6. Simulated and observed surface wind fields around 1200 UTC: surface wind speed for (a) FinalYSU and (b) FinalMYJ; (c) H*WIND analysis centered at 1230 UTC; (d) TCSWA analysis at 1200 UTC; azimuthal-mean profiles of total, tangential, and radial wind speeds for (e) YSU and (f) MYJ compared with the analyses; The azimuthal-mean wind speeds are also based on open exposure values.

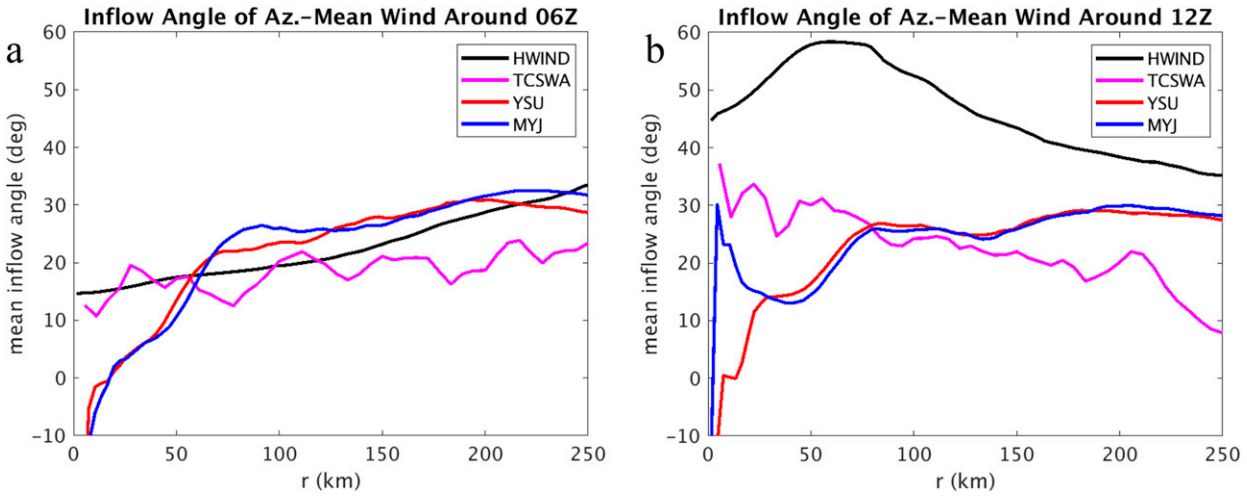

FIG. 7. Surface wind inflow angles of the azimuthal-mean simulated and analyzed surface winds at (a) 0600 UTC (0730 UTC for H*WIND and (b) 1200 UTC (1230 UTC for H*WIND).

nearly half and double the other profiles. Such differences are described by the inflow angle, defined as $\alpha = \arctan(-V_r/V_t)$. (While many previous studies do not have the negative sign, we use it here so that positive ''inflow'' means there is flow toward the center.) Zhang and Uhlhorn (2012) used hundreds of GPS dropsonde wind profiles to compute composite-mean values of α around hurricanes in the Atlantic. They found that over a wide range of intensities the mean inflow angles vary relatively little, ranging from 15° inside the RMW, increasing to 27° at 2 times the RMW, and then decreasing back to 20° at larger radii. Zhang et al. (2015) found that modifications to the boundary layer scheme in the Hurricane WRF operational forecast model (HWRF), which improved the overall structure of the boundary layer, also brought the α profiles much closer to the composite observations (and also improved forecasts of size and intensity). Wang et al. (2018) also used α to measure the positive impact of further changes to the HWRF boundary layer scheme.

Azimuthal-mean α for the simulations and analyses around 0600 UTC and 1200 UTC are shown in Fig. 7. These are inflow angles computed from the azimuthal-mean winds, not the azimuthal-means of the actual inflow angles at each grid point. The latter are very similar for H*WIND and TCSWA, but are noisier and generally 1°–5° greater for the simulations.

Over water, all of the inflow angles are similar, ranging from about 15° near the RMW to almost 30° at 250 km; TCSWA does not increase as much at large radii. Values of α for FinalYSU and FinalMYJ follow each other very closely. They also show a reversal to negative values close to $r = 0$, indicating outflow near the TC centers. As discussed above, this is probably more realistic than what is shown by H*WIND and TCSWA, which have strong inward flow all the way to the center.

Over land, the FinalYSU and FinalMYJ inflow angles are 5°–10° greater inside the RMW, but then increase to similar values of 25°–30° beyond 100 km (some of which is over water). FinalMYJ shows a spike of positive values near $r = 0$, but these are caused by highly asymmetric flows near the vortex center (not shown), and the FinalMYJ azimuthal-mean profile of α itself is very similar to the FinalYSU profile that is shown. TCSWA has larger inflow angles around the RMW. They increase further toward the center and decrease toward larger radii. H*WIND has very large inflow angles, increasing inward up to as much as 58° inside the RMW.

The strong similarities in the inflow angles of FinalYSU and FinalMYJ, over water and land, suggests they are modeling near-surface flow in ways that are at least consistent with each other. Their greater differences with TCSWA and H*WIND over land are difficult to understand, and the very large azimuthal-mean inflow angles for H*WIND seem unlikely. The topic of inflow angles will be revisited in Part II, where we will make comparisons of the simulated inflow angles with the inflow angles computed from surface observations.

4. Summary

The first goal of this study was to develop simulations of Hurricane Wilma (2005) that are sufficiently realistic so that detailed comparisons of the model output with local observations of wind speed and direction are meaningful. Fortunately, because of the large size of the storm and the strong synoptic-scale forcing involved, all of our preliminary simulations came quite close to the tracks and intensities of the real storm. Additional improvements to the storm size were made by using the vortex-bogusing technique of Rappin et al. (2013) to change the size of the initial vortex. Simulations were produced using two widely used but very different planetary boundary layer schemes: YSU and MYJ.

The model output fields were compared with the NHC ''best track'' analyses of the track and intensity of Hurricane Wilma, and with two very different objective analyses of the wind fields (H*WIND and TCSWA) before and during landfall. These comparisons show that both the FinalYSU and FinalMYJ simulations produce near-surface wind fields that are very

similar to observations. As shown in Fig. 2, from 0000 to 1800 UTC 24 October the peak surface winds are extremely close to the best-track analyses. The simulated tracks are 10 to 20 km south of the best track, but some of this difference is due to the differences between wind centers and pressure centers. The sizes of the inner-core wind fields, as measured by their respective RMWs, also fall within the range of values provided by the various observational analyses (Figs. 3 and 6).

Part II (Nolan et al. 2021) will examine the capabilities of these mesoscale simulations to reproduce overland hurricane wind fields more closely by comparing simulated surface winds at fixed points with observations at the same points. The low-level boundary layer flows will also be compared with velocity–azimuth display (VAD) analyses of the boundary layer derived from NWS Doppler radar observations (Giammanco et al. 2013). A comprehensive summary and discussion of the simulations will be provided.

Acknowledgments. The WRF simulations used in this study were produced and are archived at the University of Miami Institute for Data Science and Computing. We thank Dr. John Knaff for providing the TCSWA analyses for Hurricane Wilma, Dr. R. Fovell for providing the correction to surface wind speeds in the MYJ scheme, Dr. D. Stern for his perspective on the RI of Wilma, and Dr. R. Rotunno for comments on the paper. Authors D. Nolan and B. McNoldy were supported by the National Science Foundation under the Prediction of and Resilience Against Extreme Events (PREEVENTS) program, under Award ICER-1663947.

REFERENCES

Alapaty, K., D. Nigoyi, F. Chen, P. Pyle, A. Chandresekar, and N. Seaman, 2008: Development of the flux-adjusting surface data assimilation system for mesoscale models. *J. Appl. Meteor. Climatol.*, **47**, 2331–2350, https://doi.org/10.1175/2008JAMC1831.1.

Balderrama, J. A., and Coauthors, 2011: The Florida Coastal Monitoring Program (FCMP): A review. *J. Wind Eng. Ind. Aerodyn.*, **99**, 979–995, https://doi.org/10.1016/j.jweia.2011.07.002.

Bell, M. M., M. T. Montgomery, and K. A. Emanuel, 2012: Air–sea enthalpy and momentum exchange at major hurricane wind speeds. *J. Atmos. Sci.*, **69**, 3197–3222, https://doi.org/10.1175/JAS-D-11-0276.1.

Beven, J. L., and Coauthors, 2008: Atlantic hurricane season of 2005. *Mon. Wea. Rev.*, **136**, 1109–1173, https://doi.org/10.1175/2007MWR2074.1.

Braun, S. A., 2006: High-resolution simulation of Hurricane Bonnie (1998). Part II: Water budget. *J. Atmos. Sci.*, **63**, 43–64, https://doi.org/10.1175/JAS3609.1.

Cangialosi, J. P., 2020: National Hurricane Center Forecast Verification Report: 2019 Hurricane Season. National Hurricane Center, NOAA/NWS/Tropical Prediction Center Doc., 75 pp., https://www.nhc.noaa.gov/verification/pdfs/Verification_2019.pdf.

Cao, Y., and R. G. Fovell, 2016: Downslope windstorms of San Diego County. Part I: A case study. *Mon. Wea. Rev.*, **144**, 529–552, https://doi.org/10.1175/MWR-D-15-0147.1.

Chen, F., and J. Dudhia, 2001: Coupling an advanced land surface–hydrology model with the Penn State–NCAR MM5 modeling system. Part I: Model implementation and sensitivity. *Mon. Wea. Rev.*, **129**, 569–585, https://doi.org/10.1175/1520-0493(2001)129<0569:CAALSH>2.0.CO;2.

Chen, H., and D.-L. Zhang, 2013: On the rapid intensification of Hurricane Wilma (2005). Part II: Convective bursts and the upper-level warm core. *J. Atmos. Sci.*, **70**, 146–162, https://doi.org/10.1175/JAS-D-12-062.1.

——, ——, J. Carton, and R. Atlas, 2011: On the rapid intensification of Hurricane Wilma (2005). Part I: Model prediction and structural changes. *Wea. Forecasting*, **26**, 885–901, https://doi.org/10.1175/WAF-D-11-00001.1.

Chen, S.-S., J. F. Price, W. Zhao, M. A. Donelan, and E. J. Walsh, 2007: The CBLAST-Hurricane Program and the next-generation fully coupled atmosphere–ocean–wave models for hurricane research and prediction. *Bull. Amer. Meteor. Soc.*, **88**, 311–318, https://doi.org/10.1175/BAMS-88-3-311.

Cohen, A. E., S. M. Cavallo, M. C. Coniglio, and H. E. Brooks, 2015: A review of planetary boundary layer parameterization schemes and their sensitivity in simulating Southeastern U.S. severe weather environments. *Wea. Forecasting*, **30**, 591–612, https://doi.org/10.1175/WAF-D-14-00105.1.

Curcic, M., and B. K. Haus, 2020: Revised estimates of ocean surface drag in strong winds. *Geophys. Res. Lett.*, **47**, e2020GL087647, https://doi.org/10.1029/202GL087647.

D'Asaro, E. A., T. B. Sanford, P. P. Niiler, and E. J. Terrill, 2007: Cold wake of Hurricane Frances. *Geophys. Res. Lett.*, **34**, L15609, https://doi.org/10.1029/2007GL030160.

Davis, C., and Coauthors, 2008: Prediction of landfalling hurricanes with the Advanced Hurricane WRF Model. *Mon. Wea. Rev.*, **136**, 1990–2005, https://doi.org/10.1175/2007MWR2085.1.

DeMaria, M., and Coauthors, 2013: Improvements to the operational tropical cyclone wind speed probability model. *Wea. Forecasting*, **28**, 586–602, https://doi.org/10.1175/WAF-D-12-00116.1.

Demuth, J. L., M. DeMaria, and J. A. Knaff, 2006: Improvement of Advanced Microwave Sounding Unit tropical cyclone intensity and size estimation algorithms. *J. Appl. Meteor. Climatol.*, **45**, 1573–1581, https://doi.org/10.1175/JAM2429.1.

Deng, A., D. R. Stauffer, J. Dudhia, T. L. Otte, and G. K. Hunter, 2007: Update on analysis nudging FDDA in WRF-ARW. *Eighth WRF Users' Workshop*, Boulder, CO, WRF, 4.8, http://www2.mmm.ucar.edu/wrf/users/supports/workshop.html.

Donelan, M. A., B. K. Haus, N. Reul, W. J. Plant, M. Stiassne, H. C. Graber, O. B. Brown, and E. S. Saltzman, 2004: On the limiting aerodynamic roughness of the ocean in very strong winds. *Geophys. Res. Lett.*, **31**, L18306, https://doi.org/10.1029/2004GL019460.

Ek, M., K. Mitchell, Y. Lin, E. Rogers, P. Grunmann, E. Rogers, G. Gayno, and V. Koren, 2003: Implementation of Noah land surface model advances in the National Centers for Environmental Prediction operational mesoscale Eta. *J. Geophys. Res.*, **108**, 8851, https://doi.org/10.1029/2002JD003296.

Emanuel, K. A., 1986: An air–sea interaction theory for tropical cyclones. Part I: Steady-state maintenance. *J. Atmos. Sci.*, **43**, 585–605, https://doi.org/10.1175/1520-0469(1986)043<0585:AASITF>2.0.CO;2.

French, J. R., W. M. Drennan, J. A. Zhang, and P. G. Black, 2007: Turbulent fluxes in the hurricane boundary layer. Part I: Momentum flux. *J. Atmos. Sci.*, **64**, 1089–1102, https://doi.org/10.1175/JAS3887.1.

Gall, R., J. Franklin, F. Marks, E. N. Rappaport, and F. Toepfer, 2013: The Hurricane Forecast Improvement Project. *Bull. Amer. Meteor. Soc.*, **94**, 329–343, https://doi.org/10.1175/BAMS-D-12-00071.1.

Giammanco, I. M., J. L. Schroeder, and M. D. Powell, 2013: GPS dropwindsonde and WSR-88D observations of tropical cy-

clone vertical wind profiles and their characteristics. *Wea. Forecasting*, **28**, 77–99, https://doi.org/10.1175/WAF-D-11-00155.1.

Gregory, D., J.-J. Moncrette, C. Jakob, A. C. M. Beljaars, and T. Stockdale, 2000: Revision of convection, radiation, and cloud schemes in the ECMWF integrated forecasting system. *Quart. J. Roy. Meteor. Soc.*, **126**, 2685–2710, https://doi.org/10.1002/qj.49712656607.

Hendricks, E. A., M. S. Peng, T. Li, and X. Ge, 2011: Performance of a dynamic initialization scheme in the Coupled Ocean–Atmosphere Mesoscale Prediction System for Tropical Cyclones (COAMPS-TC). *Wea. Forecasting*, **26**, 650–663, https://doi.org/10.1175/WAF-D-10-05051.1.

Hong, S.-Y., Y. Noh, and J. Dudhia, 2006: A new vertical diffusion package with an explicit treatment of entrainment processes. *Mon. Wea. Rev.*, **134**, 2318–2341, https://doi.org/10.1175/MWR3199.1.

——, K.-S. S. Lim, Y.-H. Lee, J.-C. Ha, H.-W. Kim, S.-J. Ham, and J. Dudhia, 2010: Evaluation of the WRF double-moment 6-class microphysics scheme for precipitating convection. *Adv. Meteor.*, **2010**, 707253, https://doi.org/10.1155/2010/707253.

Iacono, M. J., J. S. Delamere, E. J. Mlawer, M. W. Shephard, S. A. Clough, and W. D. Collins, 2008: Radiative forcing by long-lived greenhouse gases: Calculations with the AER radiative transfer models. *J. Geophys. Res.*, **113**, D13103, https://doi.org/10.1029/2008JD009944.

Janjić, Z., 1994: The step-mountain eta coordinate model: Further developments of the convection, viscous sublayer, and turbulence closure schemes. *Mon. Wea. Rev.*, **122**, 927–945, https://doi.org/10.1175/1520-0493(1994)122<0927:TSMECM>2.0.CO;2.

Knabb, R. D., J. R. Rhome, and D. P. Brown, 2005: Tropical Cyclone Report: Hurricane Katrina (23–30 August 2005). NHC Tech. Rep. AL122005, 43 pp., https://www.nhc.noaa.gov/data/tcr/AL122005_Katrina.pdf.

Knaff, J. A., M. DeMaria, D. A. Molenar, C. R. Sampson, and M. G. Seybold, 2011: An automated, objective, multisatellite platform tropical cyclone surface wind analysis. *J. Appl. Meteor. Climatol.*, **50**, 2149–2166, https://doi.org/10.1175/2011JAMC2673.1.

——, S. P. Longmore, R. T. DeMaria, and D. A. Molenar, 2015: Improved tropical cyclone flight-level wind estimates using routine infrared satellite reconnaissance. *J. Appl. Meteor. Climatol.*, **54**, 463–478, https://doi.org/10.1175/JAMC-D-14-0112.1.

Kurihara, Y., M. A. Bender, and R. J. Ross, 1993: An initialization scheme of hurricane models by vortex specification. *Mon. Wea. Rev.*, **121**, 2030–2045, https://doi.org/10.1175/1520-0493(1993)121<2030:AISOHM>2.0.CO;2.

——, ——, R. E. Tuleya, and R. J. Ross, 1995: Improvements in the GFDL hurricane prediction system. *Mon. Wea. Rev.*, **123**, 2791–2801, https://doi.org/10.1175/1520-0493(1995)123<2791:IITGHP>2.0.CO;2.

Kwon, I., and H. Cheong, 2010: Tropical cyclone initialization with a spherical high-order filter and an idealized three-dimensional vortex. *Mon. Wea. Rev.*, **138**, 1344–1367, https://doi.org/10.1175/2009MWR2943.1.

Landsea, C. W., and Coauthors, 2004: The Atlantic hurricane database re-analysis project: Documentation for 1951–1910 alterations and additions to the HURDAT. *Hurricanes and Typhoons Past, Present and Future*, R. J. Murname and K.-B. Liu, Eds., Columbia University Press, 177–221.

Leslie, L. M., and G. J. Holland, 1995: On the bogussing of tropical cyclones in numerical models: A comparison of vortex profiles. *Meteor. Atmos. Phys.*, **56**, 101–110, https://doi.org/10.1007/BF01022523.

Lin, N., J. A. Smith, G. Villarini, T. P. Marchok, and M. Lynn, 2010: Modeling extreme rainfall, winds, and surge from Hurricane Isabel (2003). *Wea. Forecasting*, **25**, 1342–1361, https://doi.org/10.1175/2010WAF2222349.1.

Masters, F. J., P. J. Vickery, P. Bacon, and E. N. Rappaport, 2010: Toward objective, standardized intensity estimates from surface wind speed observations. *Bull. Amer. Meteor. Soc.*, **91**, 1665–1682, https://doi.org/10.1175/2010BAMS2942.1.

Moon, Y., and D. S. Nolan, 2010: The dynamic response of the hurricane wind field to spiral rainband heating. *J. Atmos. Sci.*, **67**, 1779–1805, https://doi.org/10.1175/2010JAS3171.1.

Morris, M., C. Chew, J. T. Reager, R. Shah, and C. Zuffada, 2019: A novel approach to monitoring wetland dynamics using CYGNSS: Everglades case study. *Remote Sens. Environ.*, **233**, 111417, https://doi.org/10.1016/j.rse.2019.111417.

National Hurricane Center, 2018: Costliest U.S. tropical cyclones tables updated. National Hurricane Center Doc., 3 pp., http://www.nhc.noaa.gov/news/UpdatedCostliest.pdf.

Nguyen, L. T., J. Molinari, and D. Thomas, 2014: Evaluation of tropical cyclone center identification methods in numerical models. *Mon. Wea. Rev.*, **142**, 4326–4339, https://doi.org/10.1175/MWR-D-14-00044.1.

Nolan, D. S., and C. Mattocks, 2014: Development and evaluation of the second hurricane nature run using the joint OSSE nature run and the WRF Model. *31st Conf. on Hurricanes and Tropical Meteorology*, San Diego, CA, Amer. Meteor. Soc., 91, https://ams.confex.com/ams/31Hurr/webprogram/Paper244751.html.

——, J. A. Zhang, and D. P. Stern, 2009a: Evaluation of planetary boundary layer parameterizations in tropical cyclones by comparison of in situ observations and high-resolution simulations of Hurricane Isabel (2003). Part I: Initialization, maximum winds, and the outer-core boundary layer. *Mon. Wea. Rev.*, **137**, 3651–3674, https://doi.org/10.1175/2009MWR2785.1.

——, D. P. Stern, and J. A. Zhang, 2009b: Evaluation of planetary boundary layer parameterizations in tropical cyclones by comparison of in situ observations and high-resolution simulations of Hurricane Isabel (2003). Part II: Inner-core boundary layer and eyewall structure. *Mon. Wea. Rev.*, **137**, 3675–3698, https://doi.org/10.1175/2009MWR2786.1.

——, R. Atlas, K. T. Bhatia, and L. R. Bucci, 2013: Development and validation of a hurricane nature run using the joint OSSE nature run and the WRF Model. *J. Adv. Model. Earth Syst.*, **5**, 382–405, https://doi.org/10.1002/jame.20031.

——, J. A. Zhang, and E. W. Uhlhorn, 2014: On the limits of estimating the maximum wind speeds in hurricanes. *Mon. Wea. Rev.*, **142**, 2814–2837, https://doi.org/10.1175/MWR-D-13-00337.1.

——, N. A. Dahl, G. H. Bryan, and R. Rotunno, 2017: Tornado vortex structure, intensity, and surface wind gusts in large-eddy simulations with fully developed turbulence. *J. Atmos. Sci.*, **74**, 1573–1597, https://doi.org/10.1175/JAS-D-16-0258.1.

——, B. D. McNoldy, J. Yunge, F. J. Masters, and I. M. Giammanco, 2021: Evaluation of the surface wind field over land in WRF simulations of Hurricane Wilma (2005). Part II: Surface winds, inflow angles, and boundary layer profiles. *Mon. Wea. Rev.*, **149**, 697–713, https://doi.org/10.1175/MWR-D-20-0201.1.

Pasch, R. J., E. S. Blake, H. D. Cobb III, and D. P. Roberts, 2006: Tropical Cyclone Report: Hurricane Wilma (15–25 October 2005). NHC Tech. Rep. AL252005, 27 pp., https://www.nhc.noaa.gov/data/tcr/AL252005_Wilma.pdf.

Pollard, R. T., P. B. Rhines, and R. O. R. Y. Thompson, 1973: The deepening of the wind-mixed layer. *Geophys. Fluid Dyn.*, **3**, 381–404, https://doi.org/10.1080/03091927208236105.

Powell, M. D., and S. H. Houston, 1996: Hurricane Andrew's landfall in South Florida. Part II: Surface wind fields and potential real-time applications. *Wea. Forecasting*, **11**, 329–349, https://doi.org/10.1175/1520-0434(1996)011<0329:HALISF>2.0.CO;2.

——, P. P. Dodge, and M. L. Black, 1991: The landfall of hurricane Hugo in the Carolinas: Surface wind distribution. *Wea. Forecasting*, **6**, 379–399, https://doi.org/10.1175/1520-0434(1991)006<0379:TLOHHI>2.0.CO;2.

——, S. H. Houston, and T. A. Reinhold, 1996: Hurricane Andrew's landfall in south Florida. Part I: Standardizing measurements for documentation of surface wind fields. *Wea. Forecasting*, **11**, 304–328, https://doi.org/10.1175/1520-0434(1996)011<0304:HALISF>2.0.CO;2.

——, ——, L. R. Amat, and N. Morisseau-Leroy, 1998: The HRD real-time hurricane wind analysis system. *J. Wind Eng. Ind. Aerodyn.*, **77–78**, 53–64, https://doi.org/10.1016/S0167-6105(98)00131-7.

——, P. J. Vickery, and T. A. Reinhold, 2003: Reduced drag coefficient for high wind speeds in tropical cyclones. *Nature*, **422**, 279–283, https://doi.org/10.1038/nature01481.

Rappin, E. D., D. S. Nolan, and S. J. Majumdar, 2013: A highly configurable vortex initialization method for tropical cyclones. *Mon. Wea. Rev.*, **141**, 3556–3575, https://doi.org/10.1175/MWR-D-12-00266.1.

Rogers, R. F., M. L. Black, S. S. Chen, and R. A. Black, 2007: An evaluation of microphysics fields from mesoscale model simulations of tropical cyclones. Part I: Comparisons with observations. *J. Atmos. Sci.*, **64**, 1811–1834, https://doi.org/10.1175/JAS3932.1.

Sampson, C. R., and J. A. Knaff, 2015: A consensus forecast for tropical cyclone gale wind radii. *Wea. Forecasting*, **30**, 1397–1403, https://doi.org/10.1175/WAF-D-15-0009.1.

——, J. S. Goerss, J. A. Knaff, B. R. Strahl, E. M. Fukada, and E. A. Serra, 2018: Tropical cyclone gale wind radii estimates, forecasts, and error forecasts for the Western North Pacific. *Wea. Forecasting*, **33**, 1081–1092, https://doi.org/10.1175/WAF-D-17-0153.1.

Skamarock, W. C., and Coauthors, 2008: A description of the Advanced Research WRF version 3. NCAR Tech. Note NCAR/TN-475+STR, 113 pp., https://doi.org/10.5065/D68S4MVH.

Stern, D. P., and D. S. Nolan, 2009: Reexamining the vertical structure of the tangential winds in tropical cyclones: Observations and theory. *J. Atmos. Sci.*, **66**, 3579–3600, https://doi.org/10.1175/2009JAS2916.1.

Takagaki, N., S. Komori, N. Suzuki, K. Iwano, T. Kuramoto, S. Shimada, R. Kurose, and K. Takahashi, 2012: Strong correlation between the drag coefficient and the shape of the wind sea spectrum over a broad range of wind speeds. *Geophys. Res. Lett.*, **39**, L23604, https://doi.org/10.1029/2012GL053988.

Uhlhorn, E. W., and D. S. Nolan, 2012: Observational undersampling and in tropical cyclones and implications for estimated intensity. *Mon. Wea. Rev.*, **140**, 825–840, https://doi.org/10.1175/MWR-D-11-00073.1.

——, P. G. Black, J. L. Franklin, M. Goodberlet, J. Carswell, and A. S. Goldstein, 2007: Hurricane surface wind measurements from an operational stepped frequency microwave radiometer. *Mon. Wea. Rev.*, **135**, 3070–3085, https://doi.org/10.1175/MWR3454.1.

Wang, W., J. A. Sippel, S. Arbaca, L. Zhu, B. Liu, Z. Zhang, A. Mehra, and V. Tallapragada, 2018: Improving NCEP HWRF simulations of surface wind and inflow angle in the eyewall area. *Wea. Forecasting*, **33**, 887–898, https://doi.org/10.1175/WAF-D-17-0115.1.

Wang, Y., L. Zhou, and K. Hamilton, 2007: Effect of convective entrainment/detrainment on the simulation of the tropical precipitation diurnal cycle. *Mon. Wea. Rev.*, **135**, 567–585, https://doi.org/10.1175/MWR3308.1.

Yablonsky, R. M., and I. Ginis, 2009: Limitation of one-dimensional ocean models for coupled hurricane–ocean model forecasts. *Mon. Wea. Rev.*, **137**, 4410–4419, https://doi.org/10.1175/2009MWR2863.1.

Zhang, J. A., and E. W. Uhlhorn, 2012: Hurricane sea surface inflow angle and an observation-based parametric model. *Mon. Wea. Rev.*, **140**, 3587–3605, https://doi.org/10.1175/MWR-D-11-00339.1.

——, D. S. Nolan, R. F. Rogers, and V. Tallapragada, 2015: Evaluating the impact of improvements in the boundary layer parameterization on hurricane intensity and structure forecasts in HWRF. *Mon. Wea. Rev.*, **143**, 3136–3155, https://doi.org/10.1175/MWR-D-14-00339.1.

Zhu, P., 2008a: Impact of land surface roughness on surface winds during hurricane landfall. *Quart. J. Roy. Meteor. Soc.*, **134**, 1051–1057, https://doi.org/10.1002/qj.265.

——, 2008b: Simulation and parameterization of the turbulent transport in the hurricane boundary layer by large eddies. *J. Geophys. Res.*, **113**, D17104, https://doi.org/10.1029/2007JD009643.